Prediction of EPR **g** Tensors in Simple d^1 Metal Porphyrins with Density Functional Theory

S. Patchkovskii and T. Ziegler*

Contribution from the Department of Chemistry, University of Calgary, 2500 University Drive NW, Calgary, Alberta, T2N 1N4 Canada

Received November 17, 1999

Abstract: Electron paramagnetic resonance (EPR) **g** tensors of 20 five- or six-coordinated d^1 metal porphyrins following the [M═E(P)]−L structural motif (M = V(IV), Nb(IV), Cr(V), Mo(V); E = N, O, S, Se; P = porphyrin dianion; L = F^-, Cl^-, Br^-, ClO_4^-, OH^-, OCH_3^-, H_2O, or not present) were computed using density functional theory (DFT). For all complexes, the singly occupied molecular orbital (SOMO) is dominated by the metal d_{xy} orbitals. Qualitative trends in $\Delta\mathbf{g}$ components are determined by magnetic-field-induced coupling of the SOMO with three classes of molecular orbitals (MOs): (a) β-spin σ MOs formed by the metal $d_{x^2-y^2}$ atomic orbital (AO) and the porphyrin ligand; (b) the corresponding vacant α-spin σ^* MOs; and (c) pairs of unoccupied α-spin π^* MOs formed between the metal d_{xz} (d_{yz}) AOs, p_x (p_y) AOs of the axial ligands, and the porphyrin π system. The rich orbital system of the porphyrin ligand usually gives rise to multiple contributions of each type. As a consequence, electronic structure of the entire porphyrin ligand must be taken into account for the analysis of experimental **g** tensors. Values of the theoretical $\Delta\mathbf{g}$ tensor components are systematically too positive compared to experiment. Once the systematic errors are accounted for, changes in the calculated **g** tensor components for complexes of metals from the same transition row are in good quantitative agreement with experiment. In oxomolybdenum porphyrinates [Mo═O(P)]−L, the sixth ligand L influences **g** tensors both through geometrical distortion of the invariant part of the complex and by direct electronic interactions. Changes in the orientation of **g** tensors upon coordination of the sixth ligand arise mostly due to the electronic effects. The importance of the direct contribution increases for more covalent ligands L. The **g** tensor components of the isolated $[Cr{=}O(P)]^+$ cation, which has not been characterized by EPR so far, are predicted to be $\Delta\mathbf{g}_\parallel = -15$ and $\Delta\mathbf{g}_\perp = -20$ ppt. The $\Delta\mathbf{g}_\parallel$ and $\Delta\mathbf{g}_\perp$ values for the $[Mo{=}O(P)]^+$ complex are predicted to be −29 and −35 ppt.

I. Introduction

Porphyrin complexes of transition metal ions play a multitude of roles in biological processes, most importantly in oxidative, photosynthetic, and transport enzymes.[1,2] In many cases, either the resting enzyme or one of the reaction intermediates contains unpaired electrons, making electron paramagnetic resonance (EPR) the tool of choice in structural and mechanistic studies of these systems.[3] So far, experimental investigations have mostly relied on the symmetry of the EPR **g** tensor and on the magnitudes of the hyperfine coupling constants in the analysis of the reaction center. The numerical values of the **g** tensor components, which contain additional information on the ligand environment, are much more difficult to interpret in terms of structural features and have been used mostly for spectral fingerprinting of the radical center.

With the development of density functional theory (DFT),[4−6] and particularly of the techniques for the calculation of EPR **g** tensors within DFT,[7−9] it became possible to provide a *quantitative* connection between the detailed molecular structure of a transition metal radical and its **g** tensor. Other theoretical approaches to the prediction of EPR **g** tensors are available in the literature, including SOS-ROHF,[10−12] MRCI,[13] MCSCF,[14] CPHF,[15] and semiempirical[16] techniques. Unfortunately, these techniques are either too computationally expensive or too unsophisticated in their treatment of electron correlation to handle a realistic model of an enzymatic reaction center, and they will not be discussed any further. In part due to the availability of inexpensive parallel computers, it is now possible to perform DFT **g** tensor calculations on systems containing more than 100 atoms. This development enables direct quantum-mechanical simulations of an accurate model of an entire enzymatic reaction center. Recently, it was shown that DFT

(1) Lippard, S. J.; Berg, J. M. *Principles of Bioinorganic Chemistry*; University Science Books: Mill Valley, California, 1994.
(2) Shelnutt, J. A.; Song, X.-Z.; Ma, J.-G.; Jentzen, S.-L.; Medforth, W. *J. Chem. Soc. Rev.* **1998**, *27*, 31.
(3) Hoff, A. J., Ed. *Advanced EPR*; Elsevier: Amsterdam, 1989.
(4) Parr, R. G.; Yang, W. *Density Functional Theory of Atoms and Molecules*; Oxford University: Oxford, 1989.
(5) Ziegler, T. *Chem. Rev.* **1991**, *91*, 651.
(6) Salahub, D. R.; Castro, M.; Proynov, E. Y. In *Relativistic and Electron Correlation Effects in Molecules and Solids*; Malli, G. L., Ed.; Plenum: New York, 1994.
(7) Schreckenbach, G.; Ziegler, T. *J. Phys. Chem. A* **1997**, *101*, 3388.
(8) van Lenthe, E.; Wormer, P. E. S.; van der Avoird, A. *J. Chem. Phys.* **1997**, *107*, 2488.
(9) Schreckenbach, G.; Ziegler, T. *Theor. Chem. Acc.* **1998**, *99*, 71.
(10) Moores, W. H.; McWeeny, R. *Proc. R. Soc. London A* **1973**, *332*, 365.
(11) Ishii, M.; Morihashi, K.; Kikuchi, O. *J. Mol. Struct. (THEOCHEM)* **1991**, *325*, 39.
(12) Lushington, G. H.; Grein, F. *Theor. Chim. Acta* **1996**, *93*, 259.
(13) Lushington, G. H.; Grein, F. *Intl. J. Quantum Chem.* **1997**, *106*, 3292.
(14) Vahtras, O.; Minaev, B.; Ågren, H. *Chem. Phys. Lett.* **1997**, *281*, 186.
(15) Jayatilaka, D. *J. Chem. Phys.* **1998**, *108*, 7587.
(16) Hsiao, Y.-W.; Zerner M. C. *Int. J. Quantum Chem.* **1999**, *75*, 577.

10.1021/ja994041a CCC: $19.00
Published on Web 03/28/2000

captures the qualitative trends in **g** tensor components stemming from major changes in the metal center and ligand environment of simple transition metal complexes.[17] Within a series of related compounds of the same transition metal ion, it is also possible to provide nearly quantitative predictions of changes in the **g** values.[17]

Enzymatic reactions, however, are often accompanied by more subtle modifications in the ligand environment, such as a conformational change in one of the ligands. It is therefore important to assess the sensitivity of the theoretical techniques to small structural changes in simple and well-characterized models before attempting to apply the theory to the interpretation of EPR spectral data in more controversial systems.

Enzymes with porphyrin-based cofactors typically include a middle or late metal ion from the first transition series, such as Mn, Fe, Co, or Cu.[1] These complexes often exhibit total spin $S > {}^1/_2$ with substantial zero-field splittings, leading to complex and difficult to interpret EPR spectra.[18] Many metal porphyrins can exist in more than one spin state, further complicating the analysis.[19] Additionally, porphyrinates of middle and late transition metals tend to be structurally flexible and may adopt any of a considerable set of "ruffled" structures depending on the environment in which they are found.[2] Accounting for vibrational and conformational averaging effects is in many cases essential[20] for obtaining a satisfactory agreement with experimental results. Although it is this type of system where theoretical calculations can potentially contribute most to the ongoing research in enzyme structure and function, a somewhat less demanding application is necessary for the initial assessment of the capabilities and accuracy of the theoretical techniques.

Several paramagnetic porphyrin complexes with the uncomplicated d^1 electronic configuration are known for early 3d and 4d transition metal ions (V(IV), Nb(IV), Cr(V), and Mo(V)). These spatially nondegenerate $S = {}^1/_2$ complexes usually exhibit simple axial or quasi-axial EPR spectra. The electronic and molecular structure of such complexes is well-understood, allowing for a direct and unambiguous comparison with theoretical predictions.

In this work, we apply DFT techniques to a series d^1 metalloporphyrins following the [M═E(P)]−L structural motif, with the porphyrin dianion (P) occupying the four equatorial positions around the metal cation M (M = V(IV), Nb(IV), Cr(V), and Mo(V)), the multiply-bound ligand E (E = O, S, Se, and N) located in one of the axial positions, and the optional L ligand (L = F^-, Cl^-, Br^-, OH^-, OCH_3^-, ClO_4^-, or water) in the second axial position. Figure 1 affords the definition of coordinate axes, notation, and the complete list of complexes considered in this study. Section II of this paper describes computational methods. Sections III and IV discuss optimized molecular geometries and theoretical **g** tensors. Section V analyzes the relative importance of geometric and electronic contributions of the ligand L for changes in the **g** tensor. Finally, section VI presents the conclusions of this investigation and provides the outlook for possible future developments.

II. Methods

All calculations are based on DFT[4−6] and were performed with the Amsterdam density functional (ADF) program package,[21−23] using Cartesian space numerical integration[24] and analytical gradients for the geometry optimization.[25,26] The implementation of the EPR **g** tensors is due to Schreckenbach and Ziegler.[7] An uncontracted triple-ζ basis of Slater-type orbitals was employed for the *n*s, *n*p, *n*d, (*n* + 1)s, and (*n* + 1)p valence shells of the transition metal elements and the *n*s and *n*p shells of the main group elements. The basis set was augmented by a set of polarization functions for main group elements and is designated as the standard basis set IV[27] in ADF. Inner shells were treated with the frozen core approximation.[22] Scalar relativistic effects were included in the quasi-relativistic framework[28] employing relativistic frozen core potentials in conjunction with the first-order Pauli Hamiltonian. Molecular geometries were optimized using the VWN[29] local density approximation (LDA) density functional. VWN LDA optimized geometries of d^1 complexes following the similar MEX_4 structural motif were previously shown to be in good agreement with experiment,[17] which is not improved with the use of the gradient-corrected BP86[30,31] functional. For all structures optimized within the constraints of the C_{4v} point group, the nature of the stationary point (a local minimum vs a saddle point) was established with normal mode vibrational analysis.[32,33] EPR **g** tensors were computed using VWN LDA as described elsewhere.[7,34] The **g** tensors of d^1 transition metal complexes were previously shown to be essentially independent of the choice of density functional.[17] All calculations, both in geometry optimization and in evaluation of the **g** tensors, employed spin-unrestricted wavefunctions.

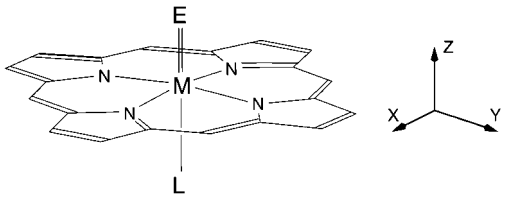

M	E	L		M	E	L	
V	O		**1**	Cr	N		**6**
V	O	H_2O	**1**-H_2O	Mo	O		**7**
V	S		**2**	Mo	O	F^-	**7**-F^-
V	Se		**3**	Mo	O	Cl^-	**7**-Cl^-
Nb	O		**4**	Mo	O	Br^-	**7**-Br^-
Nb	O	F^-	**4**-F^-	Mo	O	OH^-	**7**-OH^-
Nb	OH	F^-	**4a**-F^-	Mo	O	OCH_3^-	**7**-OCH_3^-
Cr	O		**5**	Mo	O	ClO_4^-	**7**-ClO_4^-
Cr	O	ClO_4^-	**5**-ClO_4^-	Mo	O	H_2O	**7**-H_2O
Cr	O	Cl^-	**5**-Cl^-	Mo	N		**8**

Figure 1. Molecular structure of the [M═E(P)]−L porphyrin complexes. The *Z* axis is perpendicular to the average plane of porphyrin nitrogen atoms. The *XZ* plane passes through two opposing porphyrin nitrogens.

(17) Patchkovskii, S.; Ziegler, T. *J. Chem. Phys.* **1999**, *111*, 5730.
(18) Mabbs, F. E.; Collison, D. *Electron Paramagnetic Resonance of d Transition Metal Compounds*; Elsevier: Amsterdam, 1992.
(19) Palmer, G. In *The Porphyrins*; Dolphin, D., Ed.; Academic Press: New York, 1978; Vol. IV, pp 313−353.
(20) Hagen, W. R. In *Advanced EPR*; Hoff, A. J., Ed.; Elsevier: Amsterdam, 1989; pp 785−812.
(21) ADF 2.3.3, http://tc.chem.vu.nl/SCM; Dept. of Theoretical Chemistry, Vrije Universiteit: Amsterdam.
(22) Baerends, E. J.; Ellis, D. E.; Ros, P. *Chem. Phys.* **1973**, *2*, 41.
(23) Fonseca Guerra, C.; Visser, O.; Snijders, J. G.; te Velde, G.; Baerends, E. J. In *Methods and Techniques in Computational Chemistry METECC-95*; Clementi, E., Corongiu, G., Eds.; STEF: Cagliari, 1995; pp 305−395.
(24) te Velde, G.; Baerends, E. J. *J. Comput. Chem.* **1992**, *9*, 84.
(25) Versluis, L.; Ziegler, T. *J. Chem. Phys.* **1988**, *88*, 322.
(26) Schreckenbach, G.; Li, J.; Ziegler, T. *Intl. J. Quantum Chem. Symp.* **1995**, *56*, 477.
(27) All standard ADF basis sets are available on the Internet at http://www.scm.com/Doc/atomicdata/.
(28) Ziegler, T.; Tschinke, V.; Baerends, E. J.; Snijders, J. G.; Ravenek, W. *J. Phys. Chem.* **1989**, *93*, 3050.
(29) Vosko, S. H.; Wilk, L.; Nusair, M. Can. *J. Phys.* **1980**, *58*, 1200.
(30) Becke, A. D. *Phys. Rev. A* **1988**, *38*, 3098.
(31) Perdew, J. P. *Phys. Rev. B* **1986**, *33*, 8822; **1986**, *34*, 7406.
(32) Wilson, E. B.; Decius, J. C.; Cross, P. C. *Molecular Vibrations*; Dover: New York; 1980.
(33) Fan, L.; Ziegler, T. *J. Phys. Chem.* **1992**, *96*, 6937.
(34) Schreckenbach, G. Relativity and Magnetic Properties. A Density Functional Study. Ph.D. Thesis, Univesity of Calgary, 1996.

The quasi-relativistic DFT formulation of the EPR **g** tensors used in this work distinguishes between several contributions to the **g** tensor:[7,34]

$$g_{st} = g_e\delta_{st} + \Delta g_{st}^{\mathrm{Rel}} + \Delta g_{st}^{\mathrm{d}} + \Delta g_{st}^{\mathrm{p}} \quad (1)$$

where g_e is the free electron g value ($g_e \approx 2.0023$[35]) and δ_{st} is Kronecker delta. $\Delta g_{st}^{\mathrm{Rel}}$ combines relativistic corrections arising from the kinetic energy, mass-velocity, and Darwin terms in the quasi-relativistic Hamiltonian.[34,36]

In eq 1, the terms $\Delta g_{st}^{\mathrm{d}}$ and $\Delta g_{st}^{\mathrm{p}}$ are respectively dia- and paramagnetic contributions to the **g** tensor. The paramagnetic term $\Delta g_{st}^{\mathrm{p}}$, which dominates deviation of **g** from the free electron value for complexes considered here, in turn contains contributions due to the frozen core ($\Delta g_{st}^{\mathrm{p,core}}$) as well as from the magnetic-field-induced coupling between occupied orbitals ($\Delta g_{st}^{\mathrm{p,occ-occ}}$) and between occupied and virtual orbitals ($\Delta g_{st}^{\mathrm{p,occ-vir}}$):

$$\Delta g_{st}^{\mathrm{p}} = \Delta g_{st}^{\mathrm{p,core}} + \Delta g_{st}^{\mathrm{p,occ-occ}} + \Delta g_{st}^{\mathrm{p,occ-vir}} \quad (2)$$

The term $\Delta g_{st}^{\mathrm{p,occ-vir}}$ is usually the most qualitatively important paramagnetic contribution and is given by (atomic units)

$$\Delta g_{st}^{\mathrm{p,occ-vir}} = \frac{g'}{2c}\left\{\int \frac{\partial V_{\mathrm{eff}}(\vec{\mathrm{r}})}{\partial \vec{r}}(\vec{J}_{\alpha}^{s}(\vec{r}) - \vec{J}_{\beta}^{s}(\vec{r}))\,\mathrm{d}\vec{r}\right\}_t \quad (3)$$

where $g' = 2g_e - 2 \approx 2.0046$, c is the speed of light ($c \approx 137.04$[36]), V_{eff} is the effective potential experienced by the electrons, and $\vec{J}_{\alpha}^{s}$ and $\vec{J}_{\beta}^{s}$ are the currents of respectively α- and β-spin electrons induced by a unit magnetic field B_s acting in the direction of coordinate axis s ($s = x, y, z$).

The spin-current density for spin γ ($\gamma = \alpha, \beta$) arising from the coupling between occupied and virtual molecular orbitals (MOs) induced by the external magnetic field $\vec{B}_0$ is given by

$$\vec{J}_{\gamma} = \sum_{s=1}^{3}\vec{J}_{\gamma}^{s}B_{0,s} = \sum_{s=1}^{3}\sum_{i}^{\mathrm{occ}^{\gamma}}\sum_{a}^{\mathrm{virt}^{\gamma}} u_{ai}^{s,\gamma}\{\Psi_i^{\gamma}\vec{\nabla}\Psi_a^{\gamma} - \Psi_a^{\gamma}\nabla\vec{\Psi}_i^{\gamma}\}B_{0,s} \quad (4)$$

where Ψ_i and Ψ_a are respectively occupied and virtual unperturbed Kohn−Sham orbitals and $u_{ai}^{s,\gamma}$ is the magnetic coupling coefficient between MOs i and a. The principal contribution to $u_{ai}^{s,\gamma}$ is given by[34,37]

$$u_{ai}^{s,\gamma} \approx \frac{1}{2c(\epsilon_a^{\gamma} - \epsilon_i^{\gamma})}\sum_{\nu\lambda} c_{\lambda a}^{\gamma}\, c_{\nu i}^{\gamma}\langle\chi_{\lambda}|[\vec{r}_{\nu}\times\vec{\nabla}]_s|\,\chi_{\nu}\rangle = \frac{1}{2c(\epsilon_a^{\gamma} - \epsilon_i^{\gamma})}\langle\Psi_a^{\gamma}|\hat{M}_s|\Psi_i^{\gamma}\rangle \quad (5)$$

where ϵ_a^{γ} and ϵ_i^{γ} are orbital energies of the unperturbed MOs a and i and $c_{\lambda a}^{\gamma}$ and $c_{\nu i}^{\gamma}$ are the unperturbed MO coefficients for the atomic orbitals (AOs) χ_{λ} and χ_{ν}, respectively. Matrix element $\langle\Psi_a^{\gamma}|\hat{M}_s|\Psi_i^{\gamma}\rangle$ represents the first-order magnetic coupling between an occupied molecular orbital i and a virtual orbital a. Within the GIAO formalism, the action of the magnetic coupling operator $\hat{M}_s$ on Ψ_i is simply to apply $i\hat{L}_s^{\nu}$ to each atomic orbital χ_{ν} ($\hat{L}_s^{\nu}$ is the orbital momentum operator centered at ν).

(35) Wertz, J. E.; Bolton, J. R. *Electron Spin Resonance*; Chapman and Hall: New York, 1986.

(36) Harriman, J. E. *Theoretical Foundations of Electron Spin Resonance*; Academic Press: New York, 1978.

(37) Schreckenbach, G.; Ziegler, T. *J. Phys. Chem.* **1995**, *99*, 606.

Qualitative analysis of the general equations 1−5 can be considerably simplified if α and β MOs and corresponding orbital energies are constrained to be identical (spin-restricted approach). In this case, coupling coefficients for α and β MOs become identical according to eq 4. All contributions to $\vec{J}_{\alpha}^{s}$ and $\vec{J}_{\beta}^{s}$ involving couplings between doubly occupied and fully vacant MOs in eq 3 also become numerically the same, so that the corresponding terms for $\Delta g_{st}^{\mathrm{p,occ-vir}}$ in eq 3 identically cancel. The only surviving spin-restricted contributions to $\Delta g_{st}^{\mathrm{p,occ-vir}}$ involve coupling between the α singly occupied molecular orbital (α-SOMO, Ψ_S^{α}) and virtual α MOs, as well as coupling between occupied β MOs and the (unoccupied) β-SOMO. The expression for $\Delta g_{st}^{\mathrm{p,occ-vir}}$ is then simplified to

$$\Delta g_{st}^{\mathrm{p,occ-vir}}\,(\mathrm{restricted}) = \frac{g'}{c}\sum_{a}^{\mathrm{virt}} u_{a,S}^{s} \times \left\langle\Psi_S^{\alpha}\left|\left(\frac{\partial V_{\mathrm{eff}}(\vec{r})}{\partial\vec{r}}\times\nabla\right)_t\right|\Psi_a\right\rangle - \frac{g'}{c}\sum_{i}^{\mathrm{occ}} u_{S,i}^{s}\left\langle\Psi_i\left|\left(\frac{\partial V_{\mathrm{eff}}(\vec{r})}{\partial\vec{r}}\times\nabla\right)_t\right|\Psi_S^{\beta}\right\rangle \quad (6)$$

The first sum in eq 6 arises from the magnetic-field-induced coupling between the α-SOMO and α virtual MOs and runs over all fully unoccupied MOs. The second sum runs over all doubly occupied MOs and represents the coupling of occupied β MOs with the half-empty β-SOMO. It should be emphasized that eq 6 represents only the leading term in the complete Δg_{st} expression (1). It ignores spin-polarization effects, relativistic contributions apart from the spin−orbit coupling, all core and occupied space terms, and diamagnetic and gauge invariance terms.[7,34,36] It should therefore be used only as a qualitative tool in pursuing chemical understanding of the trends in **g** shifts rather than for quantitative predictions.

The operator $\partial V_{\mathrm{eff}}/\partial\vec{r}\times\vec{\nabla}$ appearing in eq 6 is, apart from a constant, the spin-reduced form of the spin−orbit (SO) term in the first-order Pauli Hamiltonian. Matrix elements of this operator are primarily determined by one-center contributions from atom-like regions surrounding the nuclei. The spin−orbit coupling on a nucleus N will then be approximately proportional to the product of the MO coefficients due to AO contributions from the atom N in the MOs connected by the matrix element.

From eqs 5 and 6, in order to give a sizable contribution to the **g** tensor, an MO must satisfy three conditions: (a) it must have an energy close to the energy of the SOMO, so that the denominator in eq 5 is small; (b) the matrix element of the orbital momentum operator $\hat{M}$ (eq 5) between the MO and the SOMO must be large, so that the two orbitals can be coupled efficiently by the magnetic field; and (c) the spin−orbit matrix element (eq 6) between the orbitals must also be large.

III. Optimized Molecular Geometries

The key features of the optimized molecular geometries of complexes **1**−**8** are summarized in Table 1, in comparison with the available experimental data. Following the trend observed for d^1 MEX_4 complexes,[17] optimized M═E bond lengths ($R_{\mathrm{M=E}}$ in Table 1) tend to be somewhat too long, with the largest deviations from experiment found for oxomolybdenum complex **7**-F^- (VWN, 1.72 Å; exptl, 1.68 Å) and nitridomolybdenum compound **8** (VWN, 1.67 Å; exptl, 1.63 Å). The only case where theoretical M═E bond length is too short compared to experiment is the nitridochromium porphyrinate **6** (VWN, 1.54 Å; exptl, 1.57 Å).

In all structures, the transition metal ion is displaced from the mean porphyrin plane "up" toward the E-ligand (Figure 1),

Table 1. Selected Geometrical Parameters[a] of d^1 [M═E(P)]−L (P = porphyrinato) Complexes in Comparison with Experimental Values

						$R_{M=E}$, Å		ΔM, Å		$\alpha_{M=E}$, deg		R_{M-L}, Å		
	M	E	L	*z*	symm[b]	VWN	exptl	VWN	exptl	VWN	exptl	VWN	exptl	ref
1	V	O		0	C_{4v}	1.588	1.582	0.502	0.492	0.0	1.4			40
							1.652		0.534		0.0			43
1-H_2O	V	O	H_2O	0	$\approx C_s$	1.593		0.406		0.9		2.450		
2	V	S		0	C_{4v}	2.041		0.488		0.0				
3	V	Se		0	C_{4v}	2.171		0.480		0.0				
4	Nb	O		0	$\approx C_s$[c]	1.735		0.679		3.5				
4-F^-	Nb	O	F^-	−1	C_1[c]	1.773		0.234		15.1		2.042		
4a-F^-	Nb	OH	F^-	0	C_1[c]	1.920		0.150		7.6		1.930		
5	Cr	O		+1	C_{4v}	1.552		0.456		0.0				
5-ClO_4^-	Cr	O	ClO_4^-	0	C_1	1.567		0.236		1.3		2.087		
5-Cl	Cr	O	Cl^-	0	C_{4v}	1.581		0.133		0.0		2.323		
6	Cr	N		0	C_{4v}	1.535	1.565	0.393	0.421	0.0	1.6			41
7	Mo	O		+1	C_{4v}	1.686	1.67	0.569	0.66	0.0	0.0			46
7-F^-	Mo	O	F^-	0	C_{4v}	1.723	1.677	0.199	0.155	0.0	0.0	1.984	1.967	39
7-Cl^-	Mo	O	Cl^-	0	C_{4v}	1.716	1.714	0.209	0.390	0.0	0.0	2.097	2.118	51
7-Br^-	Mo	O	Br^-	0	C_{4v}	1.714		0.224		0.0		2.662		
7-OH^-	Mo	O	OH^-	0	$\approx C_s$	1.731	(1.721)	0.130	(0.130)	12.6	(0.0)	1.990	(1.951)	38[d]
7-OCH_3^-	Mo	O	OCH_3^-	0	$\approx C_s$	1.732	(1.70)	0.128	(0.20)	8.9		1.981	(1.99)	46[e]
7-ClO_4^-	Mo	O	ClO_4^-	0	$\approx C_s$	1.704		0.322		1.5		2.255		
7-H_2O	Mo	O	H_2O	+1	$\approx C_s$	1.690		0.444		0.5		2.461		
8	Mo	N		0	C_{4v}	1.674	1.630	0.494	0.548	0.0	1.7			42

[a] $R_{M=E}$ is the distance between the metal center and the multiply bound axial ligand E; ΔM is the distance between the average plane of the porphyrin nitrogens and the metal center; $\alpha_{M=E}$ is the angle between the normal to the average plane of porphyrin nitrogens and the direction of the M═E multiple bond; R_{M-L} is the distance between the metal ion and the nearest non-hydrogen atom of the ligand. [b] Point group symmetry. Geometries of complexes designated as $\approx C_s$ have been optimized within the C_1 point group. Atomic positions of the final optimized geometries were found to deviate from C_s symmetry by less than 0.002 Å. [c] The O═Nb−L fragment in this complex undergoes free rotation around the *Z* axis, see text. [d] Experimental structure for a derivative of μ-oxo-bis[(porphyrinato)oxomolybdenum(V)]. [e] Experimental structure for an $OC_6H_5^-$ complex.

both in theory and in experiment. The magnitude of the displacement (ΔM in Table 1, measured from the mean plane of the four porphyrin nitrogen atoms) is strongly dependent on the nature of the second axial ligand (L). All six-coordinated complexes are flattened compared to the parent five-coordinated compounds, with ΔM decreasing in the series L = (none) > H_2O > ClO_4^- > Br^- > Cl^- > F^- > OH^- ≈ OCH_3^-. Strongly covalent ligands (OH^-, OCH_3^-) give almost planar geometries for the metal ion−porphyrin ring part of the complex. Calculated ΔM displacements tend to be too small compared to experiment, resulting in slightly too flattened porphyrin ring geometries. The largest deviations are found in oxomolybdenum complex **7**-Cl^- (VWN, 0.21 Å; exptl, 0.39 Å) and its parent cation **7** (VWN, 0.57 Å; exptl, 0.66 Å). The experimental M−L bond lengths (R_{M-L} in Table 1) are in good agreement with the VWN results for L = F^-, Cl^-, and OCH_3^-, with errors not exceeding 0.02 Å. The apparently larger error for **7**-OH^- is due to the fact that we used the M−O bond length in chemically quite dissimilar μ-oxo-bis[(porphyrinato)oxomolybdenum(V)][38] as the "experimental" value.

Relatively large errors in calculated ΔM displacements are easily understandable given that the weakest normal vibrational mode in [M═E(P)]−L complexes usually corresponds to the motion of the E═M−L fragment along the *Z* axis, in the direction perpendicular to the porphyrin plane. This motion is coupled to the transformation between the bowl- (O═M−L in the "uppermost" position) and plate-shaped (O═M−L in the "lowermost" position) porphyrin ligands. Calculated vibrational frequencies (VWN) for this mode range from 42 cm^{-1} (for **7**-Cl^-) to 94 cm^{-1} (for **1**), corresponding to force constants in the range 20−60 kcal/mol/Å^2. With a force constant in this range, displacement of the E═M−L fragment relative to the mean porphyrin plane by 0.1 Å corresponds to a total energy change of less than 0.3 kcal/mol. As a consequence, ΔM values are likely to be sensitive to intermolecular interactions, as well as to relatively minor chemical substitutions around the porphyrin core. In the absence of crystal-packing effects restricting the motion, a weak normal mode will also result in large-amplitude thermal motion, which is evident in some experimental structures.[39] This motion can, in turn, increase the discrepancy between the static theoretical geometries and thermally averaged X-ray structures. Given both factors, the agreement between experimental and theoretical ΔM values appears to be satisfactory.

With the exception of oxoniobium porphyrinate **4**, all five-coordinated complexes (**1**−**3**, and **5**−**8**) are calculated to possess the ideal C_{4v} symmetry, with equivalent bonds between metal center and porphyrin nitrogen atoms, and the M═E moiety oriented perpendicular to the porphyrin plane. Corresponding X-ray structures are often obtained in crystal sites with lower local symmetry, so that experimental geometries of **1**,[40] **6**,[41] and **8**[42] deviate slightly from the ideal C_{4v} symmetry. The distortions are typically small, with the lengths of M−N bonds varying by up to 0.03 Å, and M═E fragments tilting by at most 2° from the normal to the porphyrin plane. In crystals where the complex occupies a site of a sufficiently high local symmetry, the ideal C_{4v} geometry is recovered, as observed for vanadyl porphyrinate.[43]

For oxoniobium(IV) porphyrinate **4**, it proved impossible to achieve an aufbau self-consistent field (SCF) solution in C_{4v} symmetry. In the $^2B_2$ electronic state, which is the ground state for this geometry, the unpaired electron occupies a molecular orbital dominated by the d_{xy} AO of the niobium atom. However, a pair of vacant e_1 MOs, derived from the π orbitals of the

(38) Kim, K.; Sparapany, J. W.; Ibers, J. A. *Acta Crystallogr. C* **1987**, *43*, 2076.
(39) Imamura, T.; Furusaki, A. *Bull. Chem. Soc. Jpn.* **1990**, *63*, 2726.
(40) Miller, S. A.; Hambley, T. W.; Taylor, J. C. *Aust. J. Chem.* **1984**, *37*, 761.
(41) Groves, J. T.; Takanashi, T.; Butler, W. M. *Inorg. Chem.* **1983**, *22*, 884.
(42) Kim, J. C.; Rees, W. S., Jr.; Goedken, V. L. *Inorg. Chem.* **1994**, *33*, 3191.
(43) Drew, M. G. B.; Mitchell, P. C. H.; Scott, C. E. *Inorg. Chim. Acta* **1984**, *82*, 63.

porphyrin ligand, then appears ca. 0.2 eV below the highest occupied molecular orbital (HOMO). This structure also corresponds to a second-order saddle point in vibrational analysis. If the unpaired electron is assigned to the e_1 MOs, giving a complex of oxoniobium(V) with a radical trianion of the porphyrin ligand, subsequent geometry optimization results in a non-aufbau SCF solution 17 kcal/mol above the $^2B_2$ state. Removing symmetry constraints in **4** and reoptimizing geometry affords a structure of an approximate C_s symmetry, with the Nb═O moiety tilted by 3° in the *XZ* plane from the *Z* axis. The MO occupations calculated for this geometry follow the aufbau principle. Because the deviation of the C_s structure from the ideal C_{4v} symmetry is relatively small, and the energy difference between the C_s and C_{4v} geometries is less than 0.5 kcal/mol, taking into account dynamical effects will likely result in effectively axial geometry for this complex.

Just as for their parent ions **5** and **7**, our calculations predict the ideal C_{4v} geometry for the six-coordinated complexes with spherically symmetric ligands L (**5**-Cl^-, **7**-F^-, **7**-Cl^-, **7**-Br^-). The E═M−L angle in these complexes is exactly 180°, and the O═M−L moiety is perpendicular to the porphyrin plane. In the two cases where X-ray structures are available (**7**-F^- and **7**-Cl^-), the complexes were found to possess C_{4v} symmetry in experiment as well.

In oxoniobium porphyrinate fluoride **4**-F^-, the O═Nb−F fragment is bent at the angle of 157°. The O═Nb bond direction is tilted by about 15° relative to the normal to the *Z* axis. The O═Nb−F fragment shows no preferred orientation in the *XY* plane and is therefore expected to undergo free rotation around the *Z* axis. **4**-F^- is the only anionic complex in the present study. This complex was characterized[44] in toluene solution, where it is likely to exist as a tightly coupled ion pair or as a protonated species, rather than as an isolated anion. In order to assess the potential influence of protonation or coordination with a countercation on the structure and EPR parameters of **4**-F^-, we examined hydroxoniobium(IV) porphyrinate fluoride **4a**-F^-, a protonated form of **4**-F^-. Upon protonation, the O═Nb−F bond angle increases to 168°, compared to 157° in the anionic complex. The Nb═O bond length increases from 1.77 Å in **4**-F^- to 1.92 Å in **4a**-F^-, indicating a decrease in the bond order between the Nb and O atoms. At the same time, the O═Nb tilt angle is reduced to 8° (15° in **4**-F^-). The motion of the HO═Nb−F fragment around the *Z* axis of the complex remains essentially free. The Nb ion moves toward the porphyrin plane by about 0.08 Å. As discussed below, these structural changes are accompanied by a profound alteration in the structure of the SOMO and in the EPR **g** tensor.

The two complexes involving a water molecule as the sixth ligand L (**1**-H_2O and **7**-H_2O) show a moderate flattening of the porphyrin ring, with the metal atom moving by about 0.1 Å toward the nitrogen plane. In both cases, the O═M−O fragment is essentially linear, with the corresponding bond angles of 176° (**1**-H_2O) and 179° (**7**-H_2O). The distances between the metal center and water oxygen are also almost identical at 2.45 Å. Given a larger radius of the Mo(V) ion, this indicates a stronger chemical bond in the charged oxomolybdenum complex. The preferred orientation of the water ligand in **1**-H_2O is with the H_2O plane almost parallel to the *XY* plane. The angle between the corresponding normals is 8°. The water molecule is bisected by the "vertical" plane passing through two opposing meso carbon atoms, giving **1**-H_2O an overall C_s symmetry. This orientation is likely the result of the electrostatic interaction between the (partially positively charged) water hydrogens and the (partially negatively charged) porphyrin nitrogen atoms. The H−N distance of ca. 2.2 Å would, however, be too large for a true hydrogen bond. In the oxomolybdenum complex **7**-H_2O, the H_2O plane is tilted by 42° relative to the *XY* porphyrin plane, so that one of the lone pairs of the water oxygen is pointed toward the molybdenum atom. In the preferred orientation of the water ligand, the H_2O plane in this complex is bisected by the *XZ* plane, also leading to the overall C_s symmetry.

The optimized geometry of the perchlorate complex *5*-ClO_4^- is unusual in the present series and shows a strong ruffling of the porphyrin core. The porphyrin ring in **5**-ClO_4^- is saddle-shaped, with an approximately C_{2v} symmetry. The σ symmetry planes pass "vertically" through the opposing pairs of the meso carbon atoms. The meso carbons, which show the largest deviation from the average plane of porphyrin nitrogens, are respectively 0.38 Å above or 0.48 Å below that plane. The ClO_4^- anion is located in the lower groove of the saddle, off-center relative to the chromium ion. The corresponding Cr−O−Cl angle is 130°. The distance between the metal center and the nearest oxygen atom of the perchlorate ion (2.09 Å) is too long to suggest a true covalent bond. The local atom arrangement around the metal center in **7**-ClO_4^- is close to the perfect axial symmetry, with the Cr═O bond direction only 1.3° from the normal to the average nitrogen plane, the O═Cr−O angle equal to 178.4°, and an 89.5° dihedral angle between two vertical planes passing through pairs of opposing nitrogen atoms. Although no experimental X-ray structure is available for **5**-ClO_4^-, the ruffled geometry of the porphyrin ligand in our calculations is supported by the EPR data, which shows a rhombic, rather than axial, spectrum for this complex.[45]

In contrast to the chromium complex **5**-ClO_4^-, its molybdenum analogue **7**-ClO_4^- is not noticeably ruffled. The porphyrin core is close to the ideal C_{4v} symmetry, and the Mo═O bond direction is tilted by just 1.5° in the *XZ* plane from the *Z* axis. The perchlorate anion is positioned with the coordinated oxygen atom on the straight line with the O═Mo bond ($\alpha_{O=Mo-O}$ = 176.9°). The chlorine atom is in the *XZ* plane underneath one of the Mo−N bonds, giving **7**-ClO_4^- an overall C_s symmetry. As for **5**-ClO_4^-, the distance between the metal center and the nearest perchlorate oxygen (2.26 Å) is too long to suggest a covalent bond.

The two oxomolybdenum complexes with a hydroxide-based ligand L (**7**-OH^- and **7**-OCH_3^-) show a very strong flattening of the porphyrin ligand. In both structures, the molybdenum atom is just 0.13 Å above the nitrogen plane, in good agreement with the available experimental values for similar complexes (0.13−0.20 Å[38,46]). Compared to 0.57 Å in the parent five-coordinated complex **7**, this is by far the largest geometry change induced by coordination of the sixth ligand. The bonds between the metal center and the oxygen atom of OH^- and OCH_3^- show a substantial covalent character, as seen from a relatively short Mo−O distance (calcd, 1.98−1.99 Å; exptl, 1.95−1.99 Å), and an increase in the axial Mo═O bond length in the trans position. In both complexes, the M═O bond direction is tilted in the *XZ* plane, by, respectively, 13° (**7**-OH^-) and 9° (**7**-OCH_3^-). The L ligand is also symmetric relative to the *XZ* plane in both compounds, giving the complexes an overall C_s symmetry. The O═Mo−O fragment is slightly closer to linearity in **7**-OCH_3^-, with a bond angle of 163° (159° in **7**-OH^-).

Overall, optimized VWN geometries appear to be in good agreement with experiment and form a reasonable starting point for calculation of EPR **g** tensors.

(44) Richard, P.; Guilard, R. *Nouv. J. Chim.* **1984**, *9*, 119.

(45) Fujii, H.; Yoshimura, T.; Kamada, H. *Inorg. Chem.* **1997**, *36*, 1122.

(46) Knorr, G.; Strähle, J. *Z. Krystallogr.* **1988**, *182*, 162.

Table 2. Calculated EPR Δ**g** Tensor Components (in Parts per Thousand, ppt) in Comparison with the Available Experimental Data

				$\Delta\mathbf{g}_{iso}$		$\Delta\mathbf{g}_{\|}$[a]		$\Delta\mathbf{g}_{\perp}$, $\Delta\mathbf{g}'_{\perp}$			
	M	E	L	VWN	exptl	VWN	exptl	VWN	exptl	solvent	ref
1	V	O		−19.5	−20	−27.6	−30	−15.4	−15	n/a (solid)	48
					−21		−38		−13	THF	47
1-H_2O	V	O	H_2O	−19.6		−26.9		−16.0			
2	V	S		−25.8	−31	−26.4	−37	−25.5	−31	unknown	52
3	V	Se		−43.8	−45	−25.5	−31	−53.0	−56	unknown	52
4	Nb	O		−22.2		(−51.8)[b]		(−16.5, +1.7)[b]			
				−22.2	−33	−33.4[c]	−55	−16.6[c]	−30	toluene	44
4-F^-	Nb	O	F^-	−19.6		(−62.8)[b]		(−7.8, +11.8)[b]			
				−19.6	(−60)[d]	−41.6[c]		−8.6[c]		toluene	44
4a-F^-	Nb	OH	F^-	−50.1		(+5.4)[b]		(−92.0, −62.8)[b]			
				−50.1		−27.1[c]		−61.6[c]			
5	Cr	O		−13.7		−9.2		−15.9			
5-ClO_4^-	Cr	O	ClO_4^-	−14.2	−20	−6.4	−16	−20.9, −15.2	−29, −20	CH_2Cl_2−toluene	45
5-Cl^-	Cr	O	Cl^-	−15.3	−20	−10.0	−16	−17.9	−22	CH_2Cl_2−toluene	45, 53
6	Cr	N		−12.6	−19.8	−28.0	−44.0	−4.9	−7.8	toluene	54
7	Mo	O		−17.0		−8.2		−21.3			
7-F^-	Mo	O	F^-	−18.1		−4.8		−24.7			
7-Cl^-	Mo	O	Cl^-	−16.6	−37.1	−3.6		−26.1		CH_2Cl_2	55
7-Br^-	Mo	O	Br^-	−19.3	−35	−2.2	(−23)[e]	−27.8	−41	CH_2Cl_2	56
7-OH^-	Mo	O	OH^-	−14.9	−34.8	−7.9		−23.3, −13.4		CH_2Cl_2	55
7-OCH_3^-	Mo	O	OCH_3^-	−14.1	−33.6	−8.5		−20.5, −13.5		CH_2Cl_2	55
					−30					toluene	57
7-ClO_4^-	Mo	O	ClO_4^-	−19.0	−39.3	−3.6		−27.1, −26.3		CH_2Cl_2	58
7-H_2O	Mo	O	H_2O	−17.7	−33	−5.9		−23.7, −23.6		acidic H_2O	59
8	Mo	N		−10.8	−28	−28.3		−2.0		toluene	42

[a] $\Delta\mathbf{g}_{\|}$ is the principal component forming the smallest angle with the *Z* axis direction (see Figure 1). [b] Principal values of the Δ**g** tensor with the internal rotation "frozen" in an arbitrary orientation. [c] Principal values of the Δ**g** tensor in the assumption of a free rotation of the E═M−L moiety within the porphyrin core, see text. [d] Experimental Δg_{iso} value reported for "**4**-F^-",[44] but likely corresponds to **4a**-F^- or a tightly coupled ion pair, see text. [e] $\Delta\mathbf{g}_{\|}$ value calculated from the experimentally measured $\Delta\mathbf{g}_{iso}$ and $\Delta\mathbf{g}_{\perp}$ values.

IV. EPR g Tensors

For the discussion of the EPR results, it is convenient to work with Δ**g** shifts, measuring the deviation of the **g** tensor from the free electron value. Δ**g** tensor is defined as

$$\Delta\mathbf{g} = \mathbf{g} - g_e\mathbf{1} \tag{7}$$

where **1** is a 3 × 3 unit matrix. Calculated Δ**g** shifts (in parts per thousand, ppt), in comparison with the available experimental data, are collected in Table 2. For complexes belonging to the C_{4v} point group (**1**, **2**, **3**, **5**, **5**-Cl^-, **6**, **7**, **7**-Cl^-, **7**-Br^-, and **8**), only two independent Δ**g** tensor components are possible by symmetry. The parallel component ($\Delta\mathbf{g}_{\|}$) is obtained when the magnetic field *B* is applied in the direction of the *Z* coordinate axis (Figure 1), parallel to the M═E bond. The doubly degenerate perpendicular component ($\Delta\mathbf{g}_{\perp}$) is observed with the magnetic field applied in an arbitrary direction within the *XY* plane. The isotropic Δ**g** shift, $\Delta\mathbf{g}_{iso}$, is then given by

$$\Delta\mathbf{g}_{iso} = (\Delta\mathbf{g}_{\|} + 2\Delta\mathbf{g}_{\perp})/3 \tag{8}$$

For the complexes with less than axial symmetry (**1**-H_2O, **5**-ClO_4^-, **7**-OH^-, **7**-OCH_3^-, **7**-$ClO4_4^-$, and **7**-H_2O), three distinct principal components are allowed. The orientation of the principal components in this case is not completely determined by symmetry. In C_s complexes (**1**-H_2O, **7**-OH^-, **7**-OCH_3^-, **7**-ClO_4^-, and **7**-H_2O), one of the components must coincide with the normal to the symmetry plane, but the orientation of the two remaining components is not determined *a priori.* In C_1 complexes, the orientation of all three principal components has to be calculated (or measured experimentally). Even so, it is useful to designate the principal component of the Δ**g** tensor forming the smallest angle with the *Z* axis bond as $\Delta\mathbf{g}_{\|}$. The two remaining components are labeled as $\Delta\mathbf{g}_{\perp}$ and $\Delta\mathbf{g}'_{\perp}$. The isotropic Δ**g** value is then given by

$$\Delta\mathbf{g}_{iso} = (\Delta\mathbf{g}_{\|} + \Delta\mathbf{g}_{\perp} + \Delta\mathbf{g}'_{\perp})/3 \tag{9}$$

The orientation of the calculated principal Δ**g** components in complexes with less than axial symmetry is given in Table 3. Unfortunately, no experimentally determined Δ**g** tensor orientations are available for these systems, so that no direct comparison with experiment is possible.

A special situation arises for the niobium(IV) complexes **4**, **4**-F^-, and **4a**-F^-. Calculated potential energy surfaces in these complexes suggest that the O═Nb−L fragment undergoes a free rotation around the *Z* axis with respect to the porphyrin ring, leading to an axial average geometry and spectral properties. The calculated EPR **g** tensors given in Table 3, on the other hand, are obtained under the assumption of a stationary molecular geometry, with the O═Nb−L fragment "frozen" in an arbitrary orientation relative to the porphyrin ring. In order to perform a meaningful comparison with experiment, calculated Δ**g** tensors in **4**, **4**-F^-, and **4a**-F^- have to be averaged, giving

$$\Delta\mathbf{g}_{\|} = \sum_{i=1}^{3} \Delta\mathbf{g}_{ii} \cos^2 \gamma_z^i \tag{10}$$

$$\Delta\mathbf{g}_{\perp} = \frac{1}{2}\sum_{i=1}^{3} \Delta\mathbf{g}_{ii} \sin^2 \gamma_z^i \tag{11}$$

where $\Delta\mathbf{g}_{ii}$ are magnitudes of the principal components of the Δ**g** tensor, while γ_z^i is the angle between the direction of the principal component *ii* and *Z* coordinate axis.

Expressions 10 and 11 would have been exact if the porphyrin ligand in **4**, **4**-F^-, and **4a**-F^- had the same C_{4v} geometry regardless of the orientation of the O═Nb−L fragment. In the presence of porphyrin relaxation, averaging would in principle require numerical integration over all possible orientations of the O═Nb−L moiety, making the calculation prohibitively

Table 3. Calculated Orientations of Δ**g** Tensor Principal Components for Non-Axially-Symmetric Complexes[a]

		direction cosines					direction cosines		
complex	$\Delta\mathbf{g}_{ii}$, ppt	*X*	*Y*	*Z*	complex	$\Delta\mathbf{g}_{ii}$, ppt	*X*	*Y*	*Z*
1-H_2O	−26.9	0.074	0.020	0.997	**7**-OH^-	−23.3	−0.005	−1.000	0.002
	−16.0	−0.358	0.934	0.008		−13.4	0.801	−0.005	−0.599
	−16.0	−0.931	−0.358	0.076		−7.9	0.599	−0.001	0.801
4[b]	−51.8	−0.582	0.006	0.813	*7*-OCH_3^-	−20.5	−0.003	−1.000	0.002
	−16.5	−0.009	−1.000	0.000		−13.5	0.885	−0.004	−0.466
	1.7	0.813	−0.008	0.582		−8.5	0.466	0.001	0.885
4-F^- [b]	−62.8	−0.455	0.267	0.850	**7**-ClO_4^-	−27.1	1.000	−0.009	0.019
	−7.8	−0.458	−0.888	0.034		−26.3	−0.009	−1.000	−0.002
	11.8	0.764	−0.373	0.526		−3.6	−0.019	−0.002	1.000
4a-F^- [b]	−93.0	−0.289	0.760	0.582	**7**-H_2O	−23.7	0.652	0.758	−0.001
	−62.8	0.938	0.346	0.013		−23.6	−0.758	0.652	0.015
	5.4	0.192	−0.550	0.813		−5.9	0.012	−0.009	1.000
5-ClO_4^-	−20.9	−0.681	0.732	0.006					
	−15.2	0.732	0.681	−0.005					
	−6.4	0.007	−0.001	1.000					

[a] See Figure 1 for the definition of coordinate axes. [b] Δ**g** tensor components for a static geometry. See text and Table 2 for the discussion of the free intramolecular rotation on the Δ**g** tensor in this complex.

expensive. However, as long as the dependence of the porphyrin ligand geometry on the O═Nb−L orientation remains small, eqs 10 and 11 provide a reasonable approximation. Axially averaged Δ**g** values for **4**, **4**-F^-, and **4a**-F^- are given in Table 2, together with the stationary rhombic values.

Correlation plots between the magnitudes of experimental and theoretical Δ**g** tensor parameters ($\Delta\mathbf{g}_{\|}$, $\Delta\mathbf{g}_{\perp}$, and $\Delta\mathbf{g}_{iso}$) are given in Figure 2. Calculated Δ**g** values are always too positive compared to experiment. The only exception is vanadyl porphyrinate **1**, for which some of the experimental values[47] appear above the calculated estimates. However, a more recent measurement on vanadyl porphyrinate crystals[48] gives principal components which essentially coincide with the theoretical result.

As previously observed for the model d^1 MEX_4^{z-} complexes,[17] the errors in the calculated Δ**g** shifts are highly systematic. The parallel component $\Delta\mathbf{g}_{\|}$ in complexes of 3d metals is overestimated by 8 ppt on average. If this value is subtracted from the theoretical results, the residual root-mean-square (RMS) error for $\Delta\mathbf{g}_{iso}$ in 3d complexes is reduced from 9.4 to 4.4 ppt (6 comparisons). In 4d complexes, the theoretical $\Delta\mathbf{g}_{\|}$ values are overestimated by 21 ppt on average. Correcting for the systematic trend reduces the residual error from 21 to less than 1 ppt (2 comparisons). Agreement with experiment is somewhat better for the perpendicular component $\Delta\mathbf{g}_{\perp}$. In 3d complexes, calculated $\Delta\mathbf{g}_{\perp}$ values are too high by 4 ppt on average (RMS(uncorrected) = 4.7, RMS(corrected) = 2.4, 7 comparisons). Again, the error is higher in 4d complexes, where theoretical $\Delta\mathbf{g}_{\perp}$ values are overestimated by about 12 ppt (RMS(uncorrected) = 13.3, RMS(corrected) = 1.3, 2 comparisons). Given the small number of experimental tensor component measurements for 4d complexes, the corrected errors are unrealistically low in these compounds. In analogy with eq 8, taking the average of the corrections for the principal components for 4d complexes gives an average systematic error for the $\Delta\mathbf{g}_{iso}$ values in the 4d systems of 15 ppt. Applying this correction to the much bigger set of $\Delta\mathbf{g}_{iso}$ values reduces the RMS error for 4d complexes from 21.4 to 9.3 ppt (9 comparisons), provided that the $\Delta\mathbf{g}_{iso}$ value of oxoniobium porphyrinate fluoride **4**-F^- is excluded. In the case of **4**-F^-, which is the only major outlier on the correlation plots, we believe that the experimental EPR signal in fact corresponds to a different chemical species (see below).

The parallels between d^1 metalloporphyrins and the model oxohalide complexes are not surprising, given the similar electronic structure of these systems. Because the comparison is important for the understanding of the qualitative origin of the Δ**g** shifts in metalloporphyrins, we shall briefly recapitulate the main contributions to Δ**g** in the model systems.[17] In the C_{4v}-symmetric MEX_4^{z-} complexes, the unpaired electron occupies a b_2 MO, dominated by the metal's d_{xy} atomic orbital. The major trends in the perpendicular component $\Delta\mathbf{g}_{\perp}$ are determined by a single term arising due to magnetic-field-induced coupling between the α-SOMO and a degenerate pair of unoccupied e_1 π-antibonding α MOs. The primary contribution to these orbitals comes from the metal's d_{xz} (d_{yz}) AO and p_x (p_y) AO of the axial ligand E. This is the "α-SOMO ↔ π*" term. The charge transfer contribution, coupling nonbonding *p*-type MOs localized on the equatorial ligands with the vacant β-SOMO, can also contribute to $\Delta\mathbf{g}_{\perp}$, but is usually not qualitatively important for light equatorial ligands. Trends in $\Delta\mathbf{g}_{\|}$ components of oxohalide complexes are determined by the interplay of two contributions of opposite signs. The negative contribution, of the "α-SOMO ↔ σ*" type, arises due to the coupling between the α-SOMO and a vacant σ-antibonding MO of b_1 symmetry. This σ* MO is formed between the metal's $d_{x^2-y^2}$ AO and an appropriate linear combination of the in-plane ligand orbitals. The positive contribution ("σ ↔ β-SOMO" type) comes from the interaction between an occupied σ-bonding β MO (b_1 symmetry) and the unoccupied β-SOMO. The σ MO involved in this term is formed from the metal's $d_{x^2-y^2}$ AO and orbitals of the equatorial ligands.

Although most of the qualitative features of the MEX_4^{z-} system are carried over to metalloporphyrins, the situation is somewhat more complicated in the latter case. The unpaired electron is again found on a molecular orbital showing large contributions from the metal d_{xy} AO, which, for C_{4v}-symmetric porphyrins, belongs to the b_2 irreducible representation. However, unlike simple halogenide anions of the model complexes, the porphyrin ligand possesses a rich π-electron system, which can interact with the the metal ion. Calculated energies of the π and π* MOs of the porphyrin ligand are close to the energy of the metal-based SOMO. This is in agreement with electrochemical data, which indicates comparable reduction potentials for the porphyrin ligand and the d^1 metal ion in many complexes of this type.[49] For some of the compounds of the more electronegative M(V) ions (**5**, **5**-ClO_4^-, **5**-Cl^-, **7**, **7**-Cl^-, **7**-Br^-,

(47) Kivelson, D.; Lee, S.-K. *J. Chem. Phys*. **1964**, *41*, 1896.
(48) Ledoux, M. J.; Michaux, O.; Hantzer, S.; Panissod, P.; Petit, P.; Andre, J.-J.; Callot, H. J. *J. Catal*. **1987**, *106*, 525.
(49) Suzuki, T.; Imamura, T.; Simiyoshi, T.; Katayama, M.; Fujimoto, M. *Inorg. Chem*. **1990**, *29*, 1123.

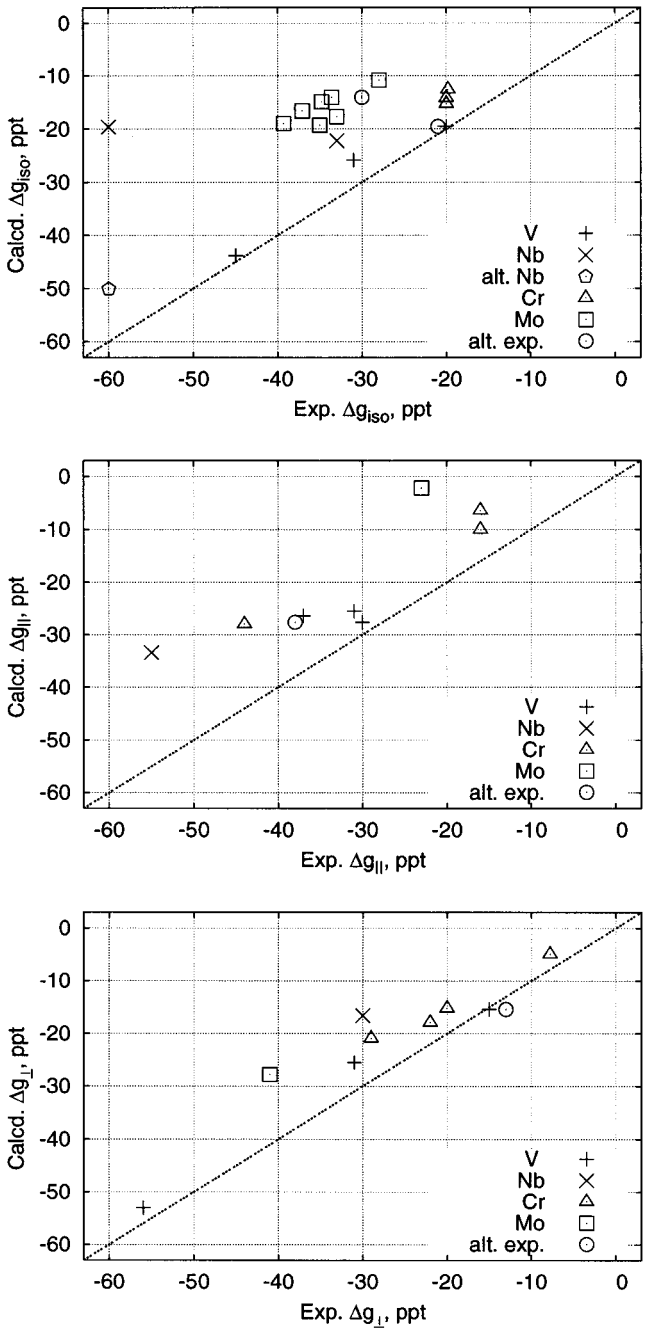

Figure 2. Calculated (VWN) $\Delta\mathbf{g}$ tensor components in comparison with experimental values. For some of the complexes (**1** and **7**-OCH_3^-), alternative experimental values have been reported in the literature. The values which we believe to be less accurate are indicated by open circles. For the niobium complex **4**, $\Delta\mathbf{g}_{||}$ and $\Delta\mathbf{g}_{\perp}$ are computed under the assumption of free rotation of the Nb═O moiety, see text. For oxoniobium compound **4**-F^-, the calculated $\Delta\mathbf{g}_{iso}$ value for an alternative protonated structure **4a**-F^- is shown with a pentagon (top panel). On each panel, the diagonal line corresponds to the perfect agreement between theory and experiment.

7-ClO_4^-, and **7**-H_2O), the doubly occupied α-spin π MOs of the porphyrin ligand in fact have higher energy than the α-SOMO. In other M(V) complexes (**6**, **7**-F^-, **7**-OH^-, **7**-OCH_3^-, and **8**), the occupied π α-MOs appear below the SOMO, as would be expected due to the destabilization of the metal d orbitals by the more covalent axial bonds in these systems. In either case, several porphyrin orbitals, both occupied and unoccupied, of symmetry needed to interact with the metal d AOs, can usually be found within a few electron-volts from

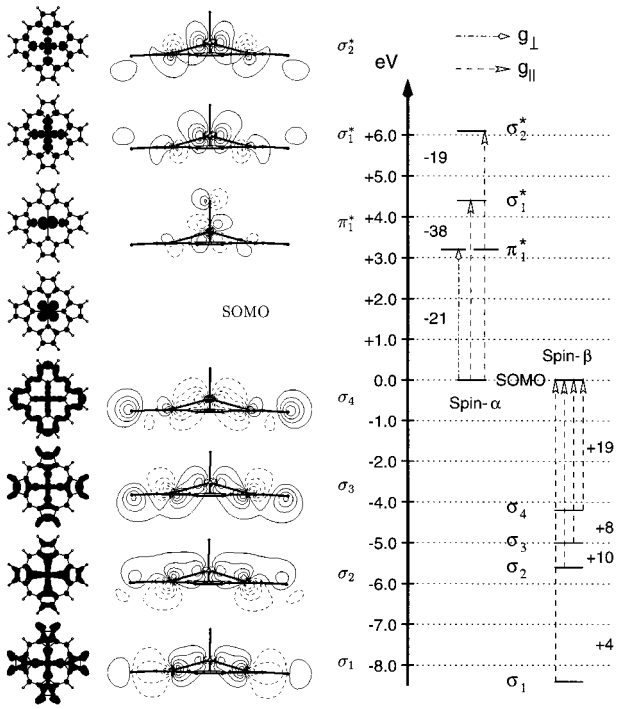

Figure 3. Principal MO contributions to the EPR $\Delta\mathbf{g}$ tensor components in **7** from a spin-unrestricted VWN calculation (rightmost panel). Contributions to $\mathbf{g}_{||}$ and $\mathbf{g}_{\perp}$ (in ppt) are indicated with dashed and dotted-dashed arrows, respectively. MO energies are given relative to the SOMO energy (spin-α, −9.30 eV; spin-β, −8.38 eV). The individual MOs are identified by the top view of the corresponding isosurface at 0.05 probability amplitude (left column) and the isolines of the cross section along the *XZ* plane (middle column). No *XZ* cross section is given for the b_2 ("d_{xy}") SOMO, which is zero by symmetry everywhere in the *XZ* plane.

the SOMO. This results in multiple terms of each type (α-SOMO ↔ π*, α-SOMO ↔ σ*, and σ ↔ β-SOMO) contributing to the $\Delta\mathbf{g}$ tensor.

As a representative example, Figure 3 shows the most important $\Delta\mathbf{g}$ contributions in oxomolybdenum porphyrinate **7**. In this complex, there are two equally important $\Delta\mathbf{g}$ contributions of the α-SOMO ↔ σ* type, giving −38 and −19 ppt, respectively. Additionally, four terms of the σ ↔ β-SOMO type contribute, respectively, +19, +10, +8, and +4 ppt to this component. The σ and σ* MOs appearing in these terms are extensively delocalized over the porphyrin ring. As the SOMO itself is strongly localized on the metal center (Mo d_{xy} AOs accounts for 95% of the SOMO in **7**), the σ ↔ β-SOMO couplings have a partial porphyrin → metal charge transfer character, while the α-SOMO ↔ σ* correspond to a partial charge transfer in the opposite direction.

A single α-spin contribution of the α-SOMO ↔ π* type dominates $\Delta\mathbf{g}_{\perp}$ in **7**. The π* MOs giving this contribution are localized on the metal center, with d_{xz} and d_{yz} metal AOs accounting for 47% of the MOs, and on the axial oxygen ligand, which accounts for 20% of the MOs via its p_x and p_y orbitals. Unlike in model MEX_4^{z-} systems, where equatorial ligands gave a negligible contribution to the π* orbitals in the α-SOMO ↔ π* term, the p_z orbitals of the porphyrin nitrogen atoms account for 8% of these MOs in **7**. From geometric considerations, the overlap between the π* M═E MOs and the porphyrin π* MOs should increase for complexes less pyramidal than **7** (see the π* MO plot in Figure 3). This, in turn, should spread the contribution of the metal d_{xz} and d_{yz} AOs over several porphyrin π* MOs, allowing them to interact efficiently with the α-SOMO

via the SO-coupling operator. Indeed, in **7**-F$^-$ ($\Delta M = 0.20$ Å, compared to $\Delta M = 0.57$ Å for **7**), two terms of the α-SOMO $\leftrightarrow \pi^*$ type contribute, respectively, −25 and −11 ppt to $\Delta\mathbf{g}_\perp$. We do not observe appreciable contributions of the charge-transfer type to $\Delta\mathbf{g}_\perp$ in the metal porphyrins. Since these contributions depend crucially on the spin−orbit coupling on the equatorial ligands, and only become important for ligands for the third main row in the model systems,[17] their absence in porphyrin complexes is hardly surprising.

Given the number of distinct contributions to the **g** tensor in the porphyrin complexes, it is imperative that any attempt at a quantitative interpretation of the values of **g** tensors in these compounds rely on the *complete* electronic structure of the complex, including the π system of the porphyrin ligand.

By far the most sizable error in the calculated $\Delta\mathbf{g}_{iso}$ values compared to experimental results is found for oxoniobium(IV) porphyrinate fluoride **4**-F$^-$. For this complex, we calculate $\Delta\mathbf{g}_{iso}$ of −20 ppt, while the experimental value reported in the literature is −60 ppt.[44] This corresponds to an error of +40 ppt, much higher than the systematic average deviation of +17 ppt found for other 4d complexes, including the parent oxoniobium(IV) porphyrinate **4**. The change in the experimental $\Delta\mathbf{g}_{iso}$ of −27 ppt between **4**-F$^-$ and **4** also appears to be unusual for d^1 porphyrin complexes, which typically change $\Delta\mathbf{g}_{iso}$ by less than 10 ppt upon insertion of the sixth ligand (see Table 2). However, the experimental EPR spectrum attributed to **4**-F$^-$, which is the only complex carrying an overall negative charge in our survey, has been measured in toluene, a medium where the existence of isolated ions is unlikely. More realistically, **4**-F$^-$ should exist in toluene either as a tightly coupled ion pair or in a protonated form, such as **4a**-F$^-$. Indeed, we calculate an isotropic $\Delta\mathbf{g}_{iso}$ value of −50 ppt for **4a**-F$^-$, 28 ppt below the calculated $\Delta\mathbf{g}_{iso}$ for **4**. Experimentally, "**4**-F$^-$" appears 27 ppt below its parent complex **4**, in almost perfect agreement with the theoretical result for **4a**-F$^-$.

The change in the calculated $\Delta\mathbf{g}_{iso}$ value between **4**-F$^-$ and **4a**-F$^-$ is primarily a result of a dramatic change in the composition of the SOMO upon protonation of the axial oxygen ligand. As illustrated in the top panel of Figure 4, the SOMO of **4a**-F$^-$ is strongly delocalized across the π system of the porphyrin ligand, with the niobium d_{xy} AOs accounting for just 36% of the SOMO. Because Nb is the heaviest nucleus in this system and accounts for the bulk of the spin−orbit coupling, low Nb contribution to the SOMO reduces the magnitude of all SO matrix elements in eq 6. The calculated $\Delta\mathbf{g}_{iso}$ shifts in **4**-F$^-$ are therefore relatively small despite the dense orbital spectrum in the vicinity of the SOMO. Protonation of the oxygen ligand in **4**-F$^-$ reduces the double character of the Nb═O bond, leading to stabilization of the niobium d orbitals, and contraction of the SOMO. As a result, the SOMO in **4a**-F$^-$ is strongly localized on the niobium atom, with the Nb d_{xy} AOs accounting for more than 83% of the SOMO (see the lower panel in Figure 4). The increased spin−orbit coupling then leads to a substantially larger absolute value of $\Delta\mathbf{g}_{iso}$. A very similar change in the Nb═O bond, the SOMO structure, and the $\Delta\mathbf{g}_{iso}$ value can be expected for a tight ion pair with a cation coordinated to the axial oxygen ligand. Therefore, this alternative also appears to be possible. However, the assignment of the signal at $\Delta\mathbf{g}_{iso} = -60$ ppt to anionic oxoniobium(IV) porphyrinate fluoride **4**-F$^-$ is clearly incompatible with our calculations.

V. The Origin of the Sixth-Ligand Influence

For the structural interpretation of EPR spectra, it is important to understand the qualitative origin of the observed changes in EPR parameters upon chemical modification of the system. Such insight is particularly helpful for processes involving labile ligands, such as axial ligand L in [M═E(P)]−L complexes. Previously, for the related molybdenum(V) oxohalide complexes, changes in the **g** tensor components upon insertion of a sixth ligand were found to arise solely from geometry relaxation for the tightly coordinated invariant ligands. Specific electronic contributions were found to be qualitatively unimportant.[50] These observations do not necessarily apply to the electronically flexible porphyrin complexes. It is therefore instructive to explicitly separate geometric and electronic influences of the sixth ligand L in our systems.

In our reference set, oxomolybdenum(V) porphyrinates [Mo═O(P)]−L have the most varied selection of experimental EPR data for different ligands L. As discussed above, our

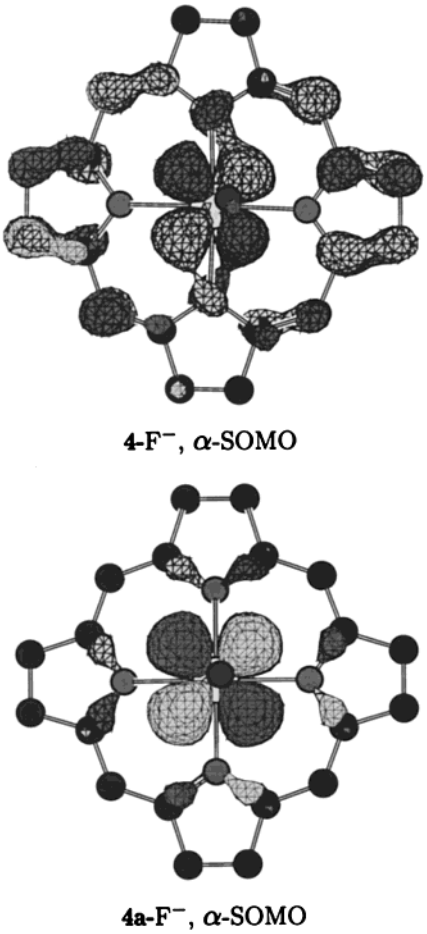

Figure 4. Composition of the α-SOMO in oxoniobium(IV)porphyrinate fluoride **4**-F$^-$ and its protonated form **4a**-F$^-$. Positions of the hydrogen atoms are omitted for clarity.

(50) Swann, J.; Westmoreland, T. D. *Inorg. Chem.* **1997**, *36*, 5348.
(51) Ledon, H.; Mentzen, B. *Inorg. Chim. Acta* **1978**, *31*, L393.
(52) Poncet, J. L.; Guilard, R.; Friant, P.; Goulon-Ginet, C.; Goulon, J. *Nouv. J. Chim.* **1984**, *8*, 583.
(53) Groves, J. T.; Haushalter, R. C. *J. Chem. Soc., Chem. Commun.* **1981**, 1165.
(54) Buchler, J. W.; Dreher, C.; Lay, K.-L.; Raap, A.; Gersonde, K. *Inorg. Chem.* **1983**, *22*, 879.
(55) Ledon, H. J.; Bonnet, M. C.; Brigandat, Y.; Varescon, F. *Inorg. Chem.* **1980**, *19*, 3488.
(56) Hasegawa, K.; Imamura, T.; Fujumoto, M. *Inorg. Chem.* **1986**, *25*, 2154.
(57) Suzuki, T.; Imamura, T.; Fujimoto, M. *Chem. Lett.* **1988**, 257.
(58) Malinski, T.; Hanley, P. M.; Kadish, K. M. *Inorg. Chem.* **1986**, *25*, 3229.
(59) Inamo, M.; Funahashi, S.; Ito, Y.; Hamada, Y.; Tanaka, M. *Chem. Lett.* **1985**, 19.

calculations are successful in reproducing changes in $\Delta\mathbf{g}_{iso}$ induced by substitution of the sixth ligand in this system. In order to separate the distinct contributions of the L ligand to $\Delta\mathbf{g}$ components, we proceed as follows: For each of the seven complexes **7**-L, we compute EPR **g** tensors twice. The first calculation, performed on the full complex at its optimized geometry, includes all terms due to the L ligand, both structural and electronic. The results of these calculations were given in Tables 2 and 3. The second calculation, performed on the [Mo═O(P)] fragment of the complex, includes the effects of structural relaxation caused by the insertion of the sixth ligand, but not the direct electronic contributions. The results of both calculations are compared in Figure 5.

Ligands L represented in Figure 5 can be separated into three categories according to their effect on $\Delta\mathbf{g}$. The only neutral ligand in our set (H_2O) and the bulky perchlorate anion show negligible direct electronic contributions and change calculated $\Delta\mathbf{g}$ values by perturbing the geometry of the invariant ligands. Coincidentally, these two ligands also show the least pronounced flattening effect on the porphyrin geometry. At the same time, ligands forming strongly covalent bonds with the molybdenum ion (OH^- and OCH_3^-) exert strong direct influence on $\Delta\mathbf{g}$. Thus, in **7**-OCH_3^-, the L-induced change in the geometry of the complex decreases $\Delta\mathbf{g}_{iso}$ by 12 ppt. However, when electronic effects of the methoxide ligand are taken into account, the total change in the calculated $\Delta\mathbf{g}_{iso}$ compared to **7** is +1.5 ppt. Therefore, direct electronic contributions of the OCH_3^- ligand to $\Delta\mathbf{g}_{iso}$ in **7**-OCH_3^- in fact increase $\Delta\mathbf{g}_{iso}$ by about 14 ppt, completely compensating the change mediated by geometry relaxation. Perhaps even more importantly, geometry change alone accounts for only 1 ppt, out of 7 ppt, of the separation between the two perpendicular components $\Delta\mathbf{g}_\perp$ and $\Delta\mathbf{g}'_\perp$ in **7**-OCH_3^-. The remaining 6 ppt arises from direct electronic effects. The orientation of the principal components is also strongly affected: in **7**-OCH_3^-, the $\Delta\mathbf{g}_\parallel$ principal component forms a 28° angle with the normal to the porphyrin plane. With the OCH_3^- ligand removed, the tilt angle drops to just 3°, making the **g** tensor almost perfectly axial.

Finally, the halogen ligands (F^-, Cl^-, and Br^-) show a behavior intermediate between the two extremal cases. Most of the change in the $\Delta\mathbf{g}_\parallel$ and $\Delta\mathbf{g}_\perp$ components in **7**-F^-, **7**-Cl^-, and **7**-Br^-, compared to the "naked" parent ion, is due to geometry relaxation. However, complexes of the individual halogen ions are differentiated from each other primarily by direct electronic contributions. As might be expected, the complex of the smallest halogenide ion (**7**-F^-) shows the most significant deviation from the purely geometric picture, while the $\Delta\mathbf{g}$ components in **7**-Br^- are much less affected by specific interactions with the Br^- ion.

Even though **g** tensors are known for five-coordinated oxovanadium(IV) and oxoniobium(IV) porphyrins, we are not aware of any experimentally measured **g** tensors for the "naked" oxochromium(V) porphyrinate cation **5** and its molybdenum analogue **7**. Although it is unlikely that "naked" **5** and **7** would exist in solution, these ions should be stable in the solid state, or in the derivatives with bulky substituents attached at the periphery of the porphyrin ligand. Given that our calculations appear to reproduce *changes* in $\Delta\mathbf{g}$ shifts upon substitution of the axial L ligand in these systems with an accuracy of a few parts per thousand, it is possible to make a prediction for the absolute $\Delta\mathbf{g}$ tensor components in **5** and **7**. From Table 2, changes in the calculated $\Delta\mathbf{g}$ values upon removal of the axial ligand from **5**-Cl^- are +1.6, +0.8, and +2.0 ppt, respectively, for $\Delta\mathbf{g}_{iso}$, $\Delta\mathbf{g}_\parallel$, and $\Delta\mathbf{g}_\perp$. Adding these Cl^- shifts to the experimental $\Delta\mathbf{g}$ values for **5**-Cl^-, we obtain the following empirically corrected EPR parameters for the "naked" cation **5**: $\Delta\mathbf{g}_{iso} = -18$ ppt, $\Delta\mathbf{g}_\parallel = -15$ ppt, and $\Delta\mathbf{g}_\perp = -20$ ppt. For oxomolybdenum(V) porphyrinates, the only full $\Delta\mathbf{g}$ tensor measurement available to us was made for **7**-Br^-. The changes in the theoretical $\Delta\mathbf{g}$ components upon removal of Br^- from **7**-Br^- are +2.3, +6.0, and +5.7 ppt, respectively, for $\Delta\mathbf{g}_{iso}$, $\Delta\mathbf{g}_\parallel$, and $\Delta\mathbf{g}_\perp$. Combining theoretical increments with the experimental $\Delta\mathbf{g}$ values for **7**-Br^-, we obtain for **7** $\Delta\mathbf{g}_{iso} = -33$ ppt, $\Delta\mathbf{g}_\parallel = -29$ ppt, and $\Delta\mathbf{g}_\perp = -35$ ppt.

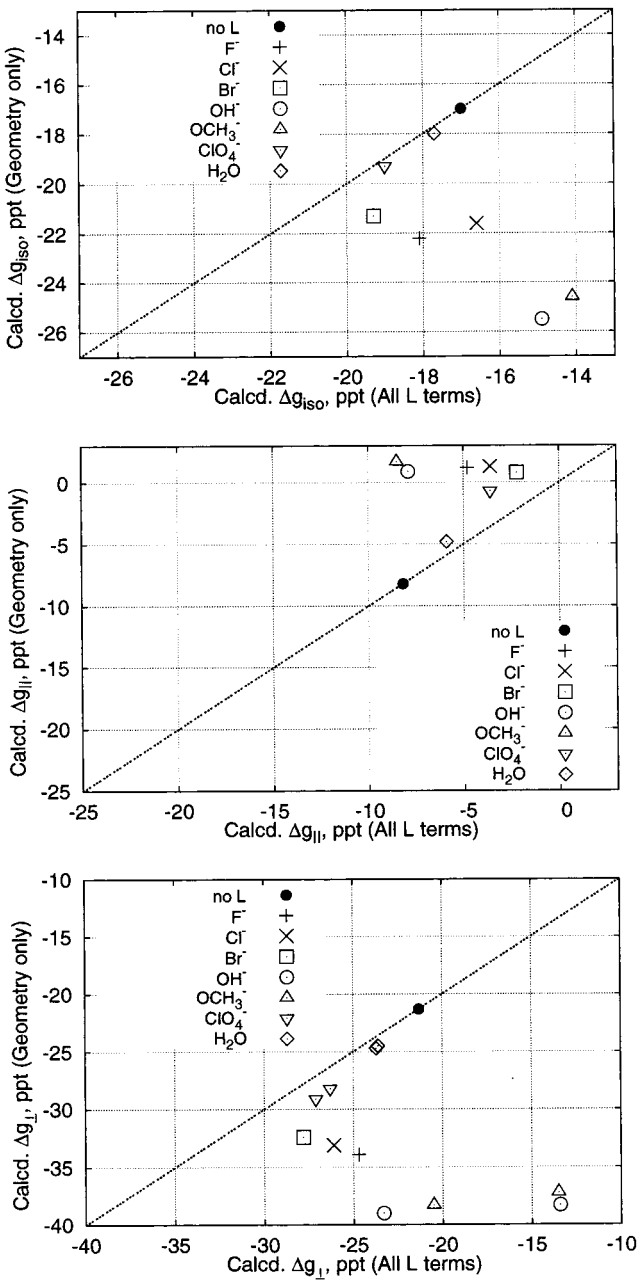

Figure 5. Direct electronic influences of the sixth ligand (L) on the **g** tensor components in [Mo═O(P)]−L oxomolybdenum(V) porphyrins. For each data point, the *X* value gives $\Delta\mathbf{g}$ shifts obtained from a full calculation on a [Mo═O(P)]−L complex. The corresponding *Y* value is computed at the same [Mo═O(P)] geometry, but with the ligand L removed. For complexes with less than axial symmetry (**7**-OH^-, **7**-OCH_3^-, **7**-ClO_4^-, and **7**-H_2O), two separate $\Delta\mathbf{g}_\perp$ values are shown. The diagonal line corresponds to negligible electronic contributions from L to $\Delta\mathbf{g}$ components.

VI. Conclusions and Outlook

In this work, we applied density functional theory to the prediction of EPR **g** tensors of five- and six-coordinated d^1 oxoporphyrinates. As in our previous study of d^1 oxohalide complexes,[17] theoretical $\Delta\mathbf{g}$ tensor components are systematically too positive compared to experiment. The parallel component $\Delta\mathbf{g}_{\|}$ is overestimated by about 8 and 21 ppt, respectively, for the 3d and 4d complexes. The corresponding average errors for $\Delta\mathbf{g}_{\perp}$ are +4 (3d) and +13 (4d) ppt. Once the systematic errors are accounted for, differences in the calculated $\Delta\mathbf{g}$ tensor components for complexes of metal ions from the same transition row agree with experiment to within a few parts per thousand.

The qualitative origin of the $\Delta\mathbf{g}$ shifts in d^1 porphyrins is similar to that in the model oxohalide compounds. The parallel component $\Delta\mathbf{g}_{\|}$ is determined by an interplay of two types of contributions. Terms arising due to the magnetic-field-induced coupling between the occupied d_{xy}-like α-SOMO and vacant σ^* MOs, formed by the metal $d_{x^2-y^2}$ AOs and equatorial ligand, are negative. Contributions to $\Delta\mathbf{g}_{\|}$ due to the coupling between occupied σ MOs, dominated by metal $d_{x^2-y^2}$ AOs and the (unoccupied) β-SOMO, are positive. The perpendicular component $\Delta\mathbf{g}_{\perp}$ is primarily determined by terms arising due to mixing between the α-SOMO and one or more pairs of degenerate π^* MOs obtained from d_{xz} and d_{yz} metal AOs. The rich π-electron system of the porphyrin ligand usually gives rise to multiple contributions of each type. As a consequence, a quantitative interpretation of experimental **g** values of d^1 metalloporphyrin complexes must take into account the electronic structure of the entire complex in order to be meaningful.

Calculations reveal two limiting types of labile axial ligands L in six-coordinated complexes. For the weakly bound neutral (H_2O) and bulky ionic (ClO_4^-) ligands, the ligand-induced change in the **g** tensor components is determined mostly by the geometrical distortion of the invariant part of the complex. For strongly covalent ligands (OH^-, OCH_3^-), both the geometry change and direct electronic effects are of equal importance and may give contributions of an opposite sign. Accounting for direct electronic influence of such ligands is essential for a qualitatively correct description of $\Delta\mathbf{g}$ shifts.

On the basis of a good correlation between the experimental and calculated isotropic $\Delta\mathbf{g}_{iso}$ shifts of six-coordinated Cr(V) and Mo(V) complexes, we predict the $\Delta\mathbf{g}$ tensor components of the isolated five-coordinated oxochromium(V) porphyrinate cation to be −15 and −20 ppt respectively for the parallel and perpendicular components. The $\Delta\mathbf{g}_{\|}$ and $\Delta\mathbf{g}_{\perp}$ values for the analogous molybdenum(V) complex are predicted to be, respectively, −29 and −35 ppt. As far as we are aware, EPR parameters have not been reported in the literature for either one of the complexes. Our calculations also suggest that the isotropic $\mathbf{g}_{iso}$ value reported[44] for the anionic oxoniobium(IV) porphyrinate fluoride **4**-F^- should be reassigned either to the neutral hydroxoniobium(IV) porphyrinate fluoride **4a**-F^- or to a tightly coupled ion pair with the countercation coordinated to the axial oxygen ligand.

Future extensions of this work may include applications to the more demanding, and less well-characterized, low-spin porphyrin complexes of manganese and iron. The ability of DFT calculations to follow reliably changes in EPR parameters stemming from chemical perturbations around the radical center can be invaluable in the interpretation of experimental results in these systems. The second possible development includes an extension of the present approach to radicals with spatially degenerate ground states, as well as the inclusion of the spin−orbit coupling terms in the second order of the perturbation theory. This will allow theoretical prediction of a complete set of EPR parameters in an arbitrary system, including radicals with the effective spin $\tilde{S} \neq {}^1/_2$. Work along these directions is currently in progress.

Acknowledgment. This work has been supported by the National Sciences and Engineering Research Council of Canada (NSERC), as well as by the donors of the Petroleum Research Fund, administered by the American Chemical Society (ACS-PRF No. 31205-AC3).

Supporting Information Available: Optimized VWN geometries of the porphyrin complexes (PDF). This material is available free of charge via the Internet at http://pubs.acs.org.

JA994041A